Metal–organic framework electrocatalysis: More than a sum of parts?

Cite as: APL Energy 1, 036106 (2023); doi: 10.1063/5.0173239
Submitted: 21 August 2023 • Accepted: 16 October 2023 •
Published Online: 9 November 2023

Alexander Bagger[1,a] and Aron Walsh[2,b]

AFFILIATIONS

[1] Department of Physics, Technical University of Denmark, Lyngby, Denmark
[2] Department of Materials, Imperial College London, London SW7 2AZ, United Kingdom

[a] Author to whom correspondence should be addressed: alexbag@dtu.dk
[b] a.walsh@imperial.ac.uk

ABSTRACT

The ever cheapening renewable energy calls for an effective means of storing and using electricity. Electrocatalysis is key for transforming electricity into chemical bonds. However, electrolysis is limited by the catalyst at the electrodes. In this work, we explore metal–organic frameworks (MOFs) as potential electrocatalysts. We investigate MOF-525, consisting of Zr nodes and tetrakis(4-carboxyphenyl)porphyrin (TCPP) linkers. We show using density functional theory simulations that metal incorporation in the ligand changes the reactivity in an electrochemical environment. Furthermore, we find that the MOF-derived porphyrin structure has a similar catalytic performance to the MOF itself for the hydrogen evolution, oxygen reduction, and CO_2 reduction reactions. Our findings highlight the challenge of using and reporting catalysis from complex hybrid materials, such as MOFs.

INTRODUCTION

Material discovery for catalysis is essential to driving forward the decarbonization of our society using the renewable energy based on wind and solar. Here, electrolysis can enable the key to store electricity in the form of chemical bonds.[1] However, electrolysis is limited by the catalyst at the electrodes, i.e., the electrocatalyst. Water electrolysis for H_2 production is an important example of an electrocatalytic process, but more exotic reactions are needed to produce our most valuable fuels and chemicals.[2] To effectively tailor electrocatalysts, advanced material discovery is required. Unfortunately, for electrocatalysis, there is an extremely challenging set of material constraints in terms of activity,[3] selectivity,[4] and stability.[5] This leaves typical electrocatalysts to be metals,[3,4] metal oxides,[5] and, recently, metal–nitrogen–carbon (MNC) structures.[6,7] The goal is to discover catalysts that fulfill these requirements and, at the same time, have radically different properties to lead to a breakthrough in the energy transition.

Metal–organic frameworks (MOFs) could lead this breakthrough by opening a new research direction in catalysis, owing to their pronounced structural differences to currently used benchmark systems. MOFs are porous solids, formed by coordination bonds between organic ligands and metal ions or clusters.[8] MOFs have been investigated for various applications because of their high porosity, internal surface area, and chemical tunability.[9] Their nanoporous structure can also give rise to an unusual electric double layer.[10] Unfortunately, MOFs with high levels of electrical conductivity are rare[11] but increasing. A mixed valence MOF with a conductivity of 1 S/cm has been demonstrated.[12] However, this is still around 100 times less than that of metal–nitrogen–carbon based materials. The electrical conductivity of MOFs, along with the chemical tunability of their active sites, has allowed the exploitation of such materials in electrocatalysis.[13,14]

Experimentally, the field of MOF electrocatalysis is growing rapidly.[15] Hod *et al.* demonstrated the activity of Fe-porphyrin-based MOFs for electroreduction of CO_2 (CO_2RR),[16] where Zn-based ZIF-8 and CALF20 acted as CO_2 to CO electrocatalysts.[17] Wang *et al.* showed close to 100% Faradaic efficiency on a Co-PMOF structure for the reaction.[18] For oxygen reduction reaction (ORR), the ZIF-8 MOF structure has been investigated by replacing Zn with Fe to achieve high and dense Fe–N_4 sites;[19,20] in addition, special MOF linker spacing in PCN-226 has been suggested to improve

the reaction kinetics,[21] and for oxygen oxidation reaction (OER), a bifunctional MOF catalyst has been reported.[22] However, one should be careful as it is not always clear if the MOF is an active catalyst or a precatalyst.[23] In the case of porphyrin-based MOFs, they could break down to active derivatives,[6,7] and in the case of bifunctional NiFe-based MOFs, they could break down to an optimal NiFe oxide catalyst.[24–26] Furthermore, it is noteworthy that metallic Zn works for CO_2 to CO electrocatalysis, challenging the observation of active ZIF-8 and CALF20 catalysts,[17] not to mention Cu-based MOFs for CO_2RR,[27] which could break down to metallic Cu particles that are known CO_2RR catalysts giving rise to a large variation of products.[2,28–32]

In this work, we highlight the use of MOFs as electrocatalysts by studying in depth MOF-525 as a template example, due to the fact that it has been studied experimentally as a working electrocatalyst for CO_2 reduction[16] and the fact that different metalations change the charge transport rate in MOF-525.[33] In addition, MOF-525 contains common features of MOFs, such as a metal node and porphyrin linker. We use density functional theory (DFT) (see the "Computational details" section), to study MOF-525 variants as depicted in Fig. 1(a). Figure 1(b) shows how the density of states for the structure changes as a function of different iron levels in the four nitrogen pockets of porphyrin. This indicates that the conductivity of this structure is a function of metal incorporation. While we acknowledge that MOF-525 could decompose to multiple different derivatives, we made the choice to construct and study two derived structures from MOF-525, which we call the TCCP molecule model [Fig. 1(c)] and the TCCP slab model [Fig. 1(d)]. This enables us to compare a MOF electrocatalytic performance with its constituent parts, and hereby estimate if the MOF and/or the degradation models are more or less active.

Fundamentally, metal and metal oxide materials are understood as catalysts.[34] The binding energies of the important reaction intermediates scale linearly[35] with each other on these surfaces, which allows for a quantification of Sabatier activity volcanoes.[36] However, these catalytic fundamental properties are not necessarily present for materials as complex as MOFs, with an organic framework and possible chemical changes during absorption.

MOF-525 contains 276 atoms, and we explore each atom as the possible binding site for *H, *COOH, *OH, *OOH, and *O intermediates to test where the catalytic intermediates bind, how strong they bind, and the effect on the electronic properties. However, we note that in certain cases, *COOH may react to form *H and CO_2 or *O reacts with the carbon framework to form *OH. These structures were discarded using a maximum distortion of 0.8 Ang.

Figure 2 depicts the matched binding energies within a 2 Ang minimum distance for MOF-525 for (a) *COOH vs *H and (b) O* vs *OH, while Fe-MOF-525 is shown in (c) *COOH vs *H and (d) *O vs *OH. The data points are colored by the DFT bandgap, and the diagonal in each plot is represented by a black dashed line. For MOF-525, it is observed that *H and *COOH adsorb strongest on the unsaturated nitrogen sites on the TCCP linker, whereas *O and *OH has binds strongest on the carbon framework, as depicted by the figure insets below the figure. For Fe-MOF-525, the Fe site is the strongest for all four intermediates, as also shown by the insets

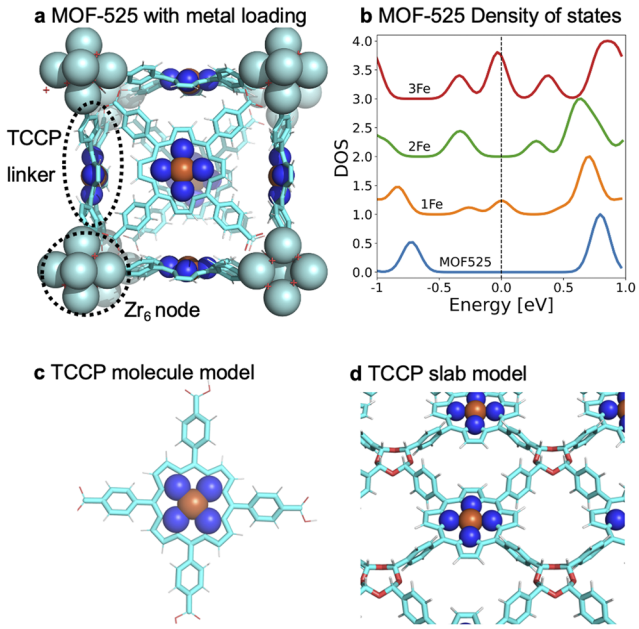

FIG. 1. (a) Structural motif of MOF-525 with an open metal site, (b) electron density of states with different amounts of Fe loading, (c) TCCP linker molecular model, and (d) TCCP slab model.

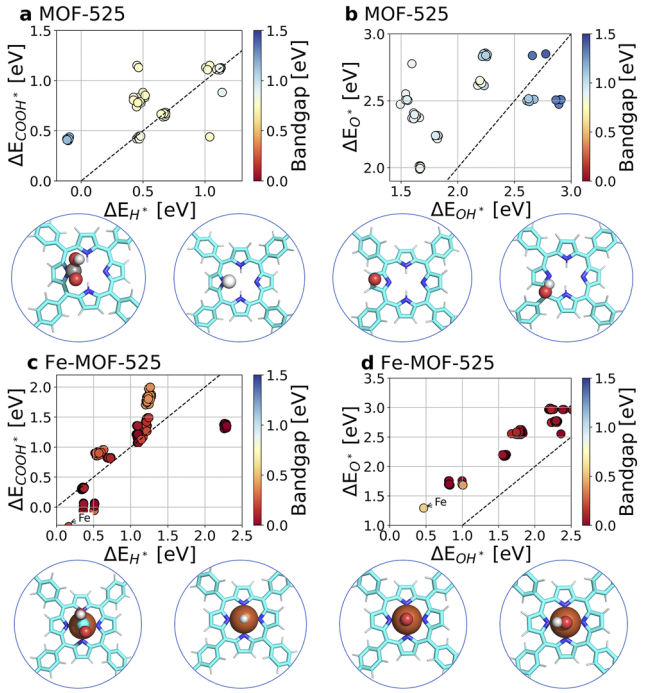

FIG. 2. Calculated scaling relations between *COOH vs *H and *O vs *OH for [(a) and (b)] MOF-525 and [(c) and (d)] Fe-MOF-525, using H_2, H_2O, and CO molecules as references. The dashed lines represent the diagonal in all plots. The structural motifs at the bottom of each panel represent the most stable *COOH, *H, *O, and *OH configurations without and with Fe.

below. Interestingly, this analysis shows a spread on the catalytic reaction intermediates that typically scale (*COOH vs *H[37] and *O vs *OH[38]). It seems that the catalytic intermediate variation on the pristine MOF-525 is larger than that on Fe-MOF-525. We believe that, in both cases, this is likely due to the formation of organic bonds that are avoided on traditional metals.

Using the MOF structure in an electrochemical setting can allow the MOF and, in particular, the metal sites (e.g., Fe) to undergo redox event or to bind/release *H, *OH, or *O species. However, it is worth noting that the MOF, due to the carbon-based structure, can directly degrade due to carbon-corrosion ($C \rightarrow CO_2$) typically observed for metal–nitrogen–carbon structures above ~0.9–1.0 V vs Reversible Hydrogen Electrode (RHE).[39,40] In our computational study, the catalytic binding intermediates in Fig. 2 can be used to study the preface behavior such as the MOF breakdown mechanism. Therefore, we study the reduction reaction

$$(H^+ + e^-) \rightarrow H^* \tag{1}$$

and several oxidation processes,

$$H^* \rightarrow (H^+ + e^-), \tag{2}$$

$$H_2O \rightarrow HO^* + (H^+ + e^-), \tag{3}$$

$$H_2O \rightarrow O^* + 2(H^+ + e^-). \tag{4}$$

We plot these reactions as a function of the electrochemical potential in Fig. 3 for (a) MOF-525 and (b) Fe-MOF-525. This allows one to interpret when, for example, *H or *OH adsorbs as a function of potential. The maximum atomic distortion is also shown, which acts as a descriptor for which reaction may lead to the decomposition of the MOF. In addition, we add red and blue regions for visualizing where the structure undergoes reduction and oxidation. In Fig. 3(a), a few *H are adsorbed close to 0 V vs Reversible Hydrogen Electrode (RHE), which is the adsorption on the unsaturated N. This adsorption leads to a minor distortion with an ~1.25 eV bandgap. Under oxidizing conditions, the initial oxidation of the structure takes place by *OH adsorbing around 1.5 V vs RHE or removing *H around 1.6 V vs RHE. We note that this intermediate oxidation is above the experimental carbon corrosion potential at 0.9–1.0 V vs RHE.[39,40] Fe-MOF-525 in Fig. 3(b) shows a different picture. The first *H

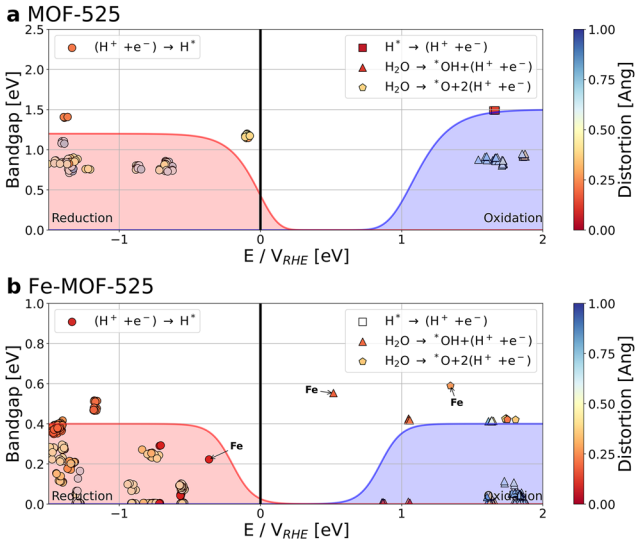

FIG. 3. MOF-525 (a) without and (b) with Fe, depicting the different reactions possible in an aqueous electrolyte as a function of potential. For visibility, a sigmoid function is added and colored to show regions where structural intermediate reduction, structural intermediate oxidation, or carbon corrosion takes place. The y-axis shows the bandgap, which is semiconducting for the pristine MOF and close to conducting with the Fe incorporation. Points are colored by the maximum distortion (Å) of the structures.

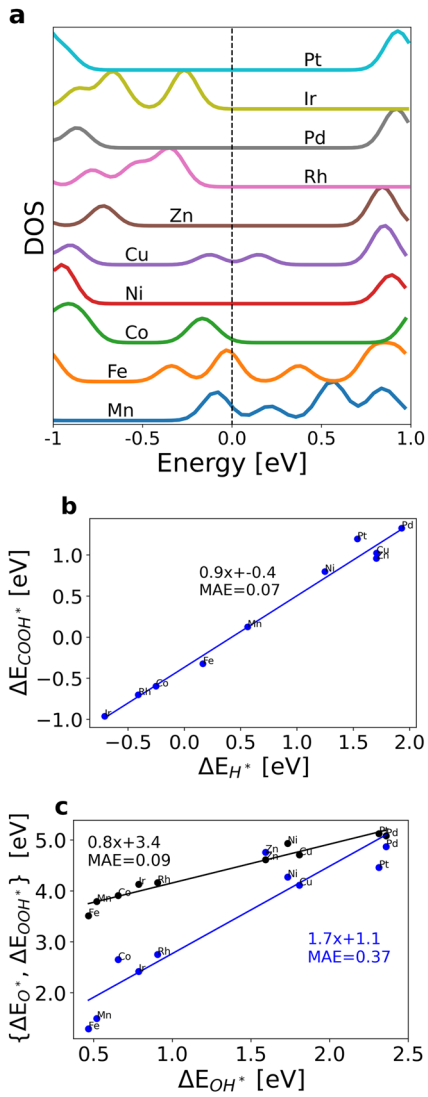

FIG. 4. MOF-525 with different amounts of metal loading. (a) Electron density of states, (b) *COOH vs *H scaling relation, and (c) *OOH and *O vs *OH scaling relations.

is adsorbed on iron at negative potentials with negligible distortions and a small bandgap. The oxidation region changes with *OH adsorption from water oxidation first taking place at Fe at ~0.5 V vs RHE. The fact that oxidizing the carbon framework still takes place at around 0.9–1.0 V vs RHE[39,40] shows that the MOF framework is probably not stable at mild oxidation potentials but could be used as a reduction reaction electrocatalyst with Fe doping.

Observing that Fe acts as an active site in MOF-525, we extend this to a series of metals (Fig. 4). Figure 4(a) shows how the density of states varies significantly around the Fermi-level (dashed line), illustrating that MOF-525 bandgap depends on metal doping and closes for certain metals. Figures 4(b) and 4(c) show that the scaling relations are intact with respect to metals. However, the slope and intersections as compared to previous work deviate, possibly due to the electronic structure. We also show the mean absolute error (MAE), which displays the simulated point errors from the line. While the MAE is low for *COOH vs *H and *OOH vs *OH (~0.1 eV), it is significantly higher for *O, possibly due to the need of pulling two electrons from the metal site as compared to one. Figure 4(b) has a slope of ~1 and intersection of −0.4, while previous results on porphyrin systems show a slope of 1 and intersection of 0.[37] The deviation in the intersection originates in the different choice of functional and CO vs using CO_2 as reference molecules, which is a known challenge in simulating CO_2RR intermediates.[41,42] The scalings shown in Figure 4(c) also deviate slightly from *OOH, *OH, and *O scalings as discussed elsewhere.[43]

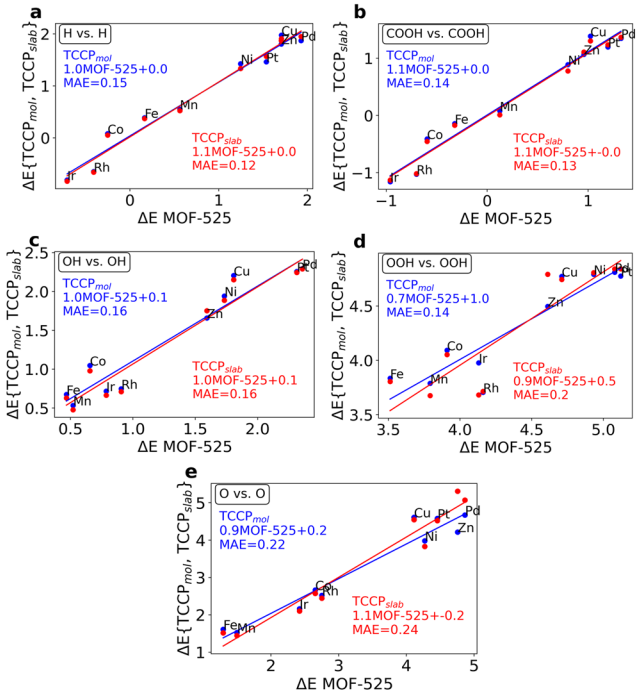

FIG. 5. Binding energy comparison of MOF-525 with a TCCP linker molecular structure (blue) and a TCCP surface slab model (red). Structural motifs are shown in Fig. 1. Direct comparison with *H, *COOH, *OH, *OOH, and *O in (a)–(e), respectively.

As MOFs could be a precatalyst[23] or simply degrade to the porphyrin motif or a derivative metal cluster, we compared DFT binding energetics of MOF-525, with a TCCP linker molecule model (blue) and a TCCP slab model (red), in Fig. 5 (see Fig. 1 for motifs). It shows that the intermediates binding at the MOF or at the derived structures are close to similar. Only a minor spread is shown on *H and *COOH intermediates in Figs. 5(a) and 5(b). For the oxygen-bound intermediates *OH, *OOH, and *O, the binding energetic spread is larger [Figs. 5(c)–5(e)], in particular for *OOH with both slope and intersection differences. This means that for oxygen reactions (i.e., ORR), there would be a catalytic activity difference depending on MOF-525 being intact during the reaction or degraded. In contrast, for Hydrogen Evolution Reaction (HER) and CO_2RR, the absolute value scatter for each metal doping on the three structures may influence the catalytic activity which we show below.

To better display the catalytic activity, the binding energies are transferred to the HER volcano [Fig. 6(a)], the ORR volcano [Fig. 6(b)], and the CO_2RR Faradaic efficiency scheme as a function of hydrogen similar to Ref. 2 [Fig. 6(c)]. When depicting the binding energies in the volcano scheme, it becomes clear that although the energetics between MOF-525 and the derived parts are linear,

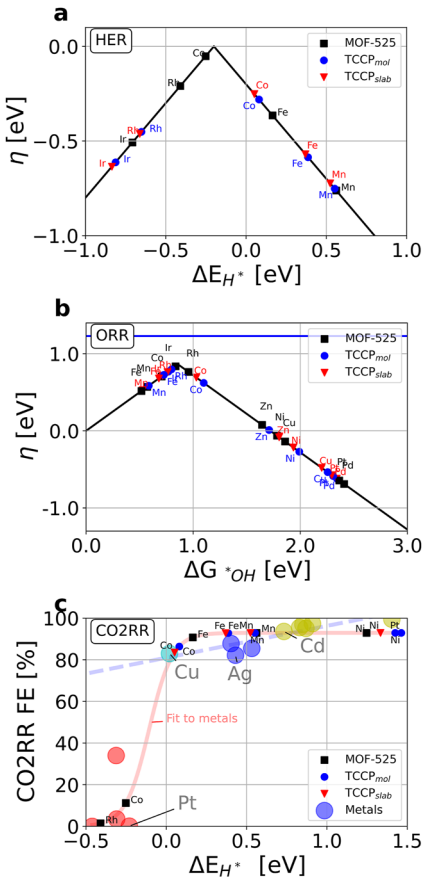

FIG. 6. (a) HER volcano, (b) ORR volcano, and (c) selectivity prediction for CO_2RR for various metals in MOF-525 and molecular TCCP hosts.

as shown in Fig. 5, their absolute value variations matter for activity and selectivity. A specific example to mention is the Co-based catalyst. For HER [Fig. 6(a)], Co-MOF-525 binds close to the top of the volcano on the strong binding side, while the degraded models bind weaker on the weak binding side of the volcano. For CO_2RR [Fig. 6(c)], which is highly sensitive to the *H binding, Co-MOF-525 binds *H strongly, giving rise to only H_2 evolution, while the degraded models are almost perfectly situated close to the calculated *H binding on metallic copper, which is known to give a series of interesting CO_2RR products.[28–32] This corresponds well to known Co compounds performing catalytically with a large variation for CO_2RR.[6,44–46] For ORR Fe-based MOFs, $TCCP_{mol}$ and $TCCP_{slab}$ structures are on the strong binding side of the volcano, which typically gives rise to four-electron ORR.[47] Fe-MOF-525 binds slightly stronger than Fe-$TCCP_{mol}$ and Fe-$TCCP_{slab}$, given the latter predicted a better activity. The Co based structures should also depend strongly on the actual structure, being that Co-MOF-525 is close to the top at the strong binding side and Co-$TCCP_{mol}$ and Co-$TCCP_{slab}$ are on the weak side, giving rise to two-electron ORR toward hydrogen peroxide. Noteworthy is that these activity schemes are based on the computational hydrogen electrode,[48] which shows activity on the reversible hydrogen electrode scale. However, it is experimentally known that the activity for molecular and M-Nx catalysts can vary as a function of pH, and it has been debated how the activity relates to the redox potential of the catalyst.[49] Computational activity prediction as a function of pH is an ongoing challenge, with the development of grand canonical approaches[50] and constant potential methods.[51] These methods are currently being employed at the electrolyte–metal interface and are beyond the scope of investigating MOFs and their derivatives. Overall, it displays that the actual structure under catalysis conditions is important for activity and selectivity.

CONCLUSION AND OUTLOOK

In summary, we have theoretically explored the electrocatalytic activity of pristine and metal-loaded MOF-525. The carbon framework allows for hydrogen (*H), hydroxyl (*OH), and oxygen (*O) adsorption from aqueous reactions in an electrochemical setup. The bandgap closes for the Fe-MOF-525 structure, and the metal becomes the active site. The incorporation of different metals on both MOF-525 and its constituents with a molecular model and a slab model of the TCCP linker shows a linear binding energy behavior. However, the absolute values of MOF-525, the TCCP molecular model, and the TCCP slab structure show changes for HER and, indeed, selectivity for CO_2RR when using predictive schemes. We suggest further experimental studies of MOFs with exposed Co and Fe sites for reduction reactions as we predict these to be conductive, electrocatalytically stable, and active catalysts.

Computational details

The MOF-525, TCCP molecule, and TCCP surface slab structures were created in the Atomic Simulation Environment (ASE).[52] For the structures, the electronic calculations were carried out with the projector augmented wave method together with the revised Perdew-Burke-Ernzerhof (RPBE) functional[53] in the GPAW software.[54,55] The MOF-525 structures were first unit cell optimized with 800 eV plane-wave mode, and the following binding energies were relaxed with a 500 eV cutoff to a force below 0.05 eV/Ang using (1 ×1× 1) k-point sampling due to the large size of cell. Spin polarized simulations were used with metal loading, and the density of states represents both spin up and spin down. For binding energies, we carry out the following calculations:

$$\Delta E_{H*} = E_{H*} - E_* - \frac{1}{2}H_2, \tag{5}$$

$$\Delta E_{COOH*} = E_{COOH*} - E_* - CO - H_2O + \frac{1}{2}H_2, \tag{6}$$

$$\Delta E_{OH*} = E_{OH*} - E_* - H_2O + \frac{1}{2}H_2. \tag{7}$$

To convert energies from ΔE to free energies (ΔG), we use a typical 0.35–0.3 = 0.05 eV correction for *OH and a 0.2 eV correction for *H. Simulation data and plotting scripts are available on https://github.com/AlexanderBagger/Metal-organic-framework-electrocatalysis-more-than-a-sum-of-parts-.

ACKNOWLEDGMENTS

A.B. acknowledges the financial support from the Carlsberg Foundation (Grant No. CF21-0144) and the Pioneer Center for Accelerating P2X Materials Discovery (CAPeX, DNRF Grant No. P3). This project was also supported with funding from Samsung Electronics Ltd. (SAIT). Via our membership of the UK's HEC Materials Chemistry Consortium, which is funded by EPSRC (Grant No. EP/X035859/1), this work used the ARCHER2 UK National Supercomputing Service (http://www.archer2.ac.uk).

AUTHOR DECLARATIONS

Conflict of Interest

The authors have no conflicts to disclose.

Author Contributions

Alexander Bagger: Conceptualization (equal); Data curation (lead); Formal analysis (lead); Funding acquisition (equal); Investigation (equal); Methodology (equal); Project administration (equal); Resources (equal); Software (equal); Validation (equal); Visualization (equal); Writing – original draft (equal); Writing – review & editing (equal). **Aron Walsh**: Conceptualization (equal); Project administration (equal); Supervision (equal); Writing – review & editing (equal).

DATA AVAILABILITY

The data that support the findings of this study are available within the article.

REFERENCES

[1] S. Chu, Y. Cui, and N. Liu, "The path towards sustainable energy," Nat. Mater. **16**, 16 (2016).
[2] I. E. L. Stephens, K. Chan, A. Bagger *et al.*, "2022 roadmap on low temperature electrochemical CO_2 reduction," J. Phys.: Energy **4**, 042003 (2022).

[3]J. N. Hansen, H. Prats, K. K. Toudahl, N. Mørch Secher, K. Chan, J. Kibsgaard, and I. Chorkendorff, "Is there anything better than Pt for HER?," ACS Energy Lett. **6**, 1175–1180 (2021).
[4]A. Bagger, W. Ju, A. S. Varela, P. Strasser, and J. Rossmeisl, "Electrochemical CO_2 reduction: A classification problem," ChemPhysChem **18**, 3266–3273 (2017).
[5]S. B. Scott, J. E. Sørensen, R. R. Rao, C. Moon, J. Kibsgaard, Y. Shao-Horn, and I. Chorkendorff, "The low overpotential regime of acidic water oxidation part II: Trends in metal and oxygen stability numbers," Energy Environ. Sci. **15**, 1988–2001 (2022).
[6]W. Ju, A. Bagger, G.-P. Hao, A. S. Varela, I. Sinev, V. Bon, B. Roldan Cuenya, S. Kaskel, J. Rossmeisl, and P. Strasser, "Understanding activity and selectivity of metal-nitrogen-doped carbon catalysts for electrochemical reduction of CO_2," Nat. Commun. **8**, 944 (2017).
[7]T. Wu, M. M. Melander, and K. Honkala, "Coadsorption of NRR and HER intermediates determines the performance of Ru-N_4 toward electrocatalytic N_2 reduction," ACS Catal. **12**, 2505–2512 (2022).
[8]S. L. James, "Metal-organic frameworks," ChemInform **34**, 276–288 (2003).
[9]R. Freund, O. Zaremba, G. Arnauts, R. Ameloot, G. Skorupskii, M. Dincă, A. Bavykina, J. Gascon, A. Ejsmont, J. Goscianska, M. Kalmutzki, U. Lächelt, E. Ploetz, C. S. Diercks, and S. Wuttke, "The current status of MOF and COF applications," Angew. Chem., Int. Ed. **60**, 23975–24001 (2021).
[10]S.-J. Shin, J. W. Gittins, M. J. Golomb, A. C. Forse, and A. Walsh, "Microscopic origin of electrochemical capacitance in metal–organic frameworks," J. Am. Chem. Soc. **145**, 14529 (2023).
[11]L. S. Xie, G. Skorupskii, and M. Dincă, "Electrically conductive metal–organic frameworks," Chem. Rev. **120**, 8536–8580 (2020).
[12]L. S. Xie, L. Sun, R. Wan, S. S. Park, J. A. DeGayner, C. H. Hendon, and M. Dincă, "Tunable mixed-valence doping toward record electrical conductivity in a three-dimensional metal–organic framework," J. Am. Chem. Soc. **140**, 7411–7414 (2018).
[13]C. A. Downes and S. C. Marinescu, "Electrocatalytic metal–organic frameworks for energy applications," ChemSusChem **10**, 4374–4392 (2017).
[14]A. Morozan and F. Jaouen, "Metal organic frameworks for electrochemical applications," Energy Environ. Sci. **5**, 9269–9290 (2012).
[15]D. Narváez-Celada and A. S. Varela, "CO_2 electrochemical reduction on metal-organic framework catalysts: Current status and future directions," J. Mater. Chem. A **10**, 5899–5917 (2022).
[16]I. Hod, M. D. Sampson, P. Deria, C. P. Kubiak, O. K. Farha, and J. T. Hupp, "Fe-porphyrin-based metal–organic framework films as high-surface concentration, heterogeneous catalysts for electrochemical reduction of CO_2," ACS Catal. **5**, 6302–6309 (2015).
[17]T. A. Al-Attas, N. N. Marei, X. Yong, N. G. Yasri, V. Thangadurai, G. Shimizu, S. Siahrostami, and M. G. Kibria, "Ligand-engineered metal–organic frameworks for electrochemical reduction of carbon dioxide to carbon monoxide," ACS Catal. **11**, 7350–7357 (2021).
[18]Y. R. Wang, Q. Huang, C. T. He, Y. Chen, J. Liu, F. C. Shen, and Y. Q. Lan, "Oriented electron transmission in polyoxometalate-metalloporphyrin organic framework for highly selective electroreduction of CO_2," Nat. Commun. **9**, 4466 (2018).
[19]L. Jiao, J. Li, L. L. Richard *et al.*, "Chemical vapour deposition of Fe–N–C oxygen reduction catalysts with full utilization of dense Fe–N_4 sites," Nat. Mater. **20**, 1385–1391 (2021).
[20]A. Mehmood, M. Gong, F. Jaouen, A. Roy, A. Zitolo, A. Khan, M.-T. Sougrati, M. Primbs, A. M. Bonastre, D. Fongalland, G. Drazic, P. Strasser, and A. Kucernak, "High loading of single atomic iron sites in Fe–NC oxygen reduction catalysts for proton exchange membrane fuel cells," Nat. Catal. **5**, 311–323 (2022).
[21]M. O. Cichocka, Z. Liang, D. Feng, S. Back, S. Siahrostami, X. Wang, L. Samperisi, Y. Sun, H. Xu, N. Hedin, H. Zheng, X. Zou, H.-C. Zhou, and Z. Huang, "A porphyrinic zirconium metal–organic framework for oxygen reduction reaction: Tailoring the spacing between active-sites through chain-based inorganic building units," J. Am. Chem. Soc. **142**, 15386–15395 (2020).
[22]W. Cheng, X. Zhao, H. Su, F. Tang, W. Che, H. Zhang, and Q. Liu, "Lattice-strained metal–organic-framework arrays for bifunctional oxygen electrocatalysis," Nat. Energy **4**, 115–122 (2019).
[23]W. Zheng and L. Y. S. Lee, "Metal-organic frameworks for electrocatalysis: Catalyst or precatalyst?," ACS Energy Lett. **6**, 2838–2843 (2021).
[24]O. Diaz-Morales, I. Ledezma-Yanez, M. T. M. Koper, and F. Calle-Vallejo, "Guidelines for the rational design of Ni-based double hydroxide electrocatalysts for the oxygen evolution reaction," ACS Catal. **5**, 5380–5387 (2015).
[25]F. Dionigi, Z. Zeng, I. Sinev, T. Merzdorf, S. Deshpande, M. B. Lopez, S. Kunze, I. Zegkinoglou, H. Sarodnik, D. Fan, A. Bergmann, J. Drnec, J. F. d. Araujo, M. Gliech, D. Teschner, J. Zhu, W. X. Li, J. Greeley, B. R. Cuenya, and P. Strasser, "In-situ structure and catalytic mechanism of NiFe and CoFe layered double hydroxides during oxygen evolution," Nat. Commun. **11**, 2522 (2020).
[26]Y. Zhou and N. López, "The role of Fe species on NiOOH in oxygen evolution reactions," ACS Catal. **10**, 6254–6261 (2020).
[27]U. Nwosu and S. Siahrostami, "Copper-based metal–organic frameworks for CO_2 reduction: Selectivity trends, design paradigms, and perspectives," Catal. Sci. Technol. **13**, 3740–3761 (2023).
[28]L. Zaza, K. Rossi, and R. Buonsanti, "Well-defined copper-based nanocatalysts for selective electrochemical reduction of CO_2 to C_2 products," ACS Energy Lett. **7**, 1284–1291 (2022).
[29]G. Kastlunger, H. H. Heenen, and N. Govindarajan, "Combining first-principles kinetics and experimental data to establish guidelines for product selectivity in electrochemical CO_2 reduction," ACS Catal. **13**, 5062–5072 (2023).
[30]J. Hussain, H. Jónsson, and E. Skúlason, "Calculations of product selectivity in electrochemical CO_2 reduction," ACS Catal. **8**, 5240–5249 (2018).
[31]R. Kortlever, J. Shen, K. J. P. Schouten, F. Calle-Vallejo, and M. T. M. Koper, "Catalysts and reaction pathways for the electrochemical reduction of carbon dioxide," J. Phys. Chem. Lett. **6**, 4073–4082 (2015).
[32]S. Asperti, R. Hendrikx, Y. Gonzalez-Garcia, and R. Kortlever, "Benchmarking the electrochemical CO_2 reduction on polycrystalline copper foils: The importance of microstructure versus applied potential," ChemCatChem **14**, e202200540 (2022).
[33]P. A. Herrera-Herrera, E. Rodríguez-Sevilla, and A. S. Varela, "The role of the metal center on charge transport rate in MOF-525: Cobalt and nickel porphyrin," Dalton Trans. **50**, 16939–16944 (2021).
[34]J. K. Nørskov, F. Studt, F. Abild-Pedersen, and T. Bligaard, *Fundamental Concepts in Heterogenous Catalysis*, 9781118888 (John Wiley & Sons, Ltd.; Wiley, 2014), pp. 1–196.
[35]F. Abild-Pedersen, J. Greeley, F. Studt, J. Rossmeisl, T. R. Munter, P. G. Moses, E. Skúlason, T. Bligaard, and J. K. Nørskov, "Scaling properties of adsorption energies for hydrogen-containing molecules on transition-metal surfaces," Phys. Rev. Lett. **99**, 016105 (2007).
[36]P. Sabatier, *La Catalyse en Chimie Organique* (Librairie Polytechnique, Paris et Liege, 1920), p. 1920.
[37]A. Bagger, W. Ju, A. Varela, P. Strasser, and J. Rossmeisl, "Single site porphyrine-like structures advantages over metals for selective electrochemical CO_2 reduction," Catal. Today **288**, 74–78 (2017).
[38]I. C. Man, H.-Y. Su, F. Calle-Vallejo, H. A. Hansen, J. I. Martínez, N. G. Inoglu, J. Kitchin, T. F. Jaramillo, J. K. Nørskov, and J. Rossmeisl, "Universality in oxygen evolution electrocatalysis on oxide surfaces," ChemCatChem **3**, 1159–1165 (2011).
[39]C. H. Choi, C. Baldizzone, G. Polymeros, E. Pizzutilo, O. Kasian, A. K. Schuppert, N. Ranjbar Sahraie, M.-T. Sougrati, K. J. J. Mayrhofer, and F. Jaouen, "Minimizing operando demetallation of Fe-N-C electrocatalysts in acidic medium," ACS Catal. **6**, 3136–3146 (2016).
[40]C. H. Choi, C. Baldizzone, J.-P. Grote, A. K. Schuppert, F. Jaouen, and K. J. J. Mayrhofer, "Stability of Fe-N-C catalysts in acidic medium studied by operando spectroscopy," Angew. Chem., Int. Ed. **54**, 12753–12757 (2015).
[41]R. Christensen, H. A. Hansen, and T. Vegge, "Identifying systematic DFT errors in catalytic reactions," Catal. Sci. Technol. **5**, 4946–4949 (2015).
[42]L. P. Granda-Marulanda, A. Rendón-Calle, S. Builes, F. Illas, M. T. M. Koper, and F. Calle-Vallejo, "A semiempirical method to detect and correct DFT-based gas-phase errors and its application in electrocatalysis," ACS Catal. **10**, 6900–6907 (2020).
[43]S. Divanis, T. Kutlusoy, I. M. Ingmer Boye, I. C. Man, and J. Rossmeisl, "Oxygen evolution reaction: A perspective on a decade of atomic scale simulations," Chem. Sci. **11**, 2943–2950 (2020).
[44]E. Boutin, M. Wang, J. C. Lin, M. Mesnage, D. Mendoza, B. Lassalle-Kaiser, C. Hahn, T. F. Jaramillo, and M. Robert, "Aqueous electrochemical reduction of

carbon dioxide and carbon monoxide into methanol with cobalt phthalocyanine," Angew. Chem. **131**, 16318–16322 (2019).
[45]M. Hossain, P. Prslja, C. Flox, N. Muthuswamy, J. Sainio, A. Kannan, M. Suominen, N. Lopez, and T. Kallio, "Temperature dependent product distribution of electrochemical CO_2 reduction on CoTPP/MWCNT composite," Appl. Catal., B **304**, 120863 (2022).
[46]Y. Wu, Z. Jiang, X. Lu, Y. Liang, and H. Wang, "Domino electroreduction of CO_2 to methanol on a molecular catalyst," Nature **575**, 639–642 (2019).
[47]A. M. Patel, S. Ringe, S. Siahrostami, M. Bajdich, J. K. Nørskov, and A. R. Kulkarni, "Theoretical approaches to describing the oxygen reduction reaction activity of single-atom catalysts," J. Phys. Chem. C **122**, 29307–29318 (2018).
[48]J. K. Nørskov, J. Rossmeisl, A. Logadottir, L. Lindqvist, J. R. Kitchin, T. Bligaard, and H. Jónsson, "Origin of the overpotential for oxygen reduction at a fuel-cell cathode," J. Phys. Chem. B **108**, 17886–17892 (2004).
[49]J. H. Zagal and M. T. Koper, "Reactivity descriptors for the activity of molecular MN4 catalysts for the oxygen reduction reaction," Angew. Chem., Int. Ed. **55**, 14510–14521 (2016).
[50]M. M. Melander, "Grand canonical ensemble approach to electrochemical thermodynamics, kinetics, and model Hamiltonians," Curr. Opin. Electrochem. **29**, 100749 (2021).
[51]G. Kastlunger, L. Wang, N. Govindarajan, H. H. Heenen, S. Ringe, T. Jaramillo, C. Hahn, and K. Chan, "Using pH dependence to understand mechanisms in electrochemical CO reduction," ACS Catal. **12**, 4344–4357 (2022).
[52]A. Hjorth Larsen, J. Jørgen Mortensen, J. Blomqvist, I. E. Castelli, R. Christensen, M. Dułak, J. Friis, M. N. Groves, B. Hammer, C. Hargus, E. D. Hermes, P. C. Jennings, P. Bjerre Jensen, J. Kermode, J. R. Kitchin, E. Leonhard Kolsbjerg, J. Kubal, K. Kaasbjerg, S. Lysgaard, J. Bergmann Maronsson *et al.*, "The atomic simulation environment—A Python library for working with atoms," J. Phys.: Condens. Matter **29**, 273002 (2017).
[53]B. Hammer, L. B. Hansen, and J. K. Nørskov, "Improved adsorption energetics within density-functional theory using revised Perdew-Burke-Ernzerhof functionals," Phys. Rev. B **59**, 7413–7421 (1999).
[54]J. J. Mortensen, L. B. Hansen, and K. W. Jacobsen, "Real-space grid implementation of the projector augmented wave method," Phys. Rev. B **71**, 035109 (2005).
[55]J. Enkovaara, C. Rostgaard, J. J. Mortensen, J. Chen, M. Dułak, L. Ferrighi, J. Gavnholt, C. Glinsvad, V. Haikola, H. A. Hansen, H. H. Kristoffersen, M. Kuisma, A. H. Larsen, L. Lehtovaara, M. Ljungberg, O. Lopez-Acevedo, P. G. Moses, J. Ojanen, T. Olsen, V. Petzold *et al.*, "Electronic structure calculations with GPAW: A real-space implementation of the projector augmented-wave method," J. Phys.: Condens. Matter **22**, 253202 (2010).